Supplementary material

Simultaneous inhibition of peripheral CB1R and iNOS mitigates obesity-related dyslipidemia through distinct mechanisms.

Célia Roger, Chloé Buch, Tania Muller, Julia Leemput, Laurent Demizieux, Patricia Passilly-Degrace, Resat Cinar, Malliga R Iyer, George Kunos, Bruno Vergès, Pascal Degrace and Tony Jourdan.

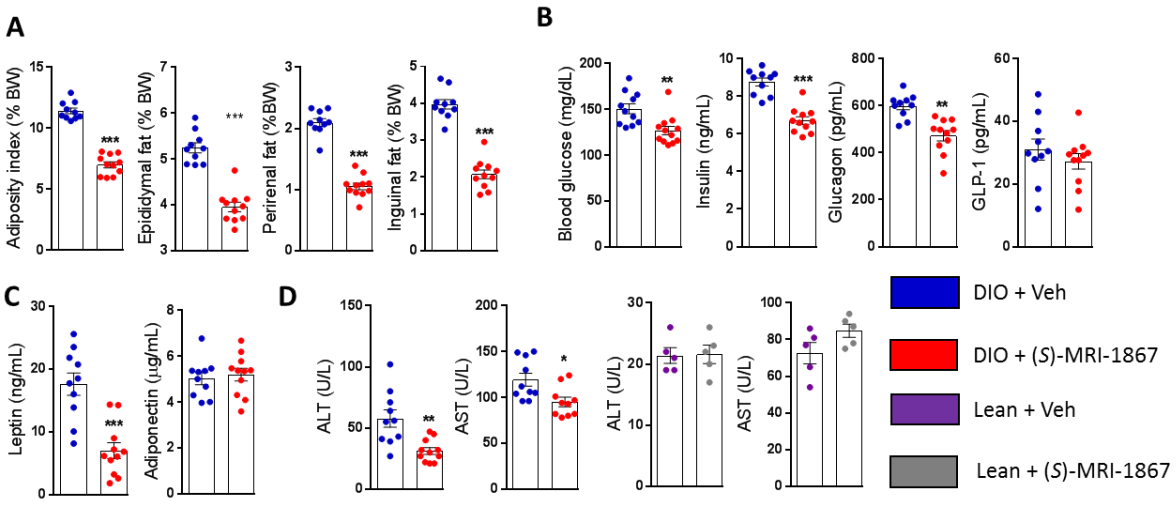

Supplementary Fig. 1: (*S*)-MRI-1867 reduced adiposity index, improves pancreatic function and restore adipokine secretion in DIO mice. (A) Adiposity index along with relative epididymal, perirenal and inguinal fat mass in DIO mice. (B) Fasting blood glucose and serum concentration of insulin, glucagon and GLP-1 in DIO mice. (C) Serum concentration of the adipokines leptin and adiponectin. (D) Serum transaminase concentrations in DIO and lean mice. Purple dots represent the lean vehicle control mice (n=5) while the grey dots represent the lean (*S*)-MRI-1867 treated mice (n=5). Blue dots represent the DIO vehicle control mice (n=10) while the red dots represent the DIO *(S)*-MRI-1867 treated mice (n=11). Data represent mean ± SEM. Significance relative to vehicle control: *p<0,05; **p<0,01; ***p<0,001.

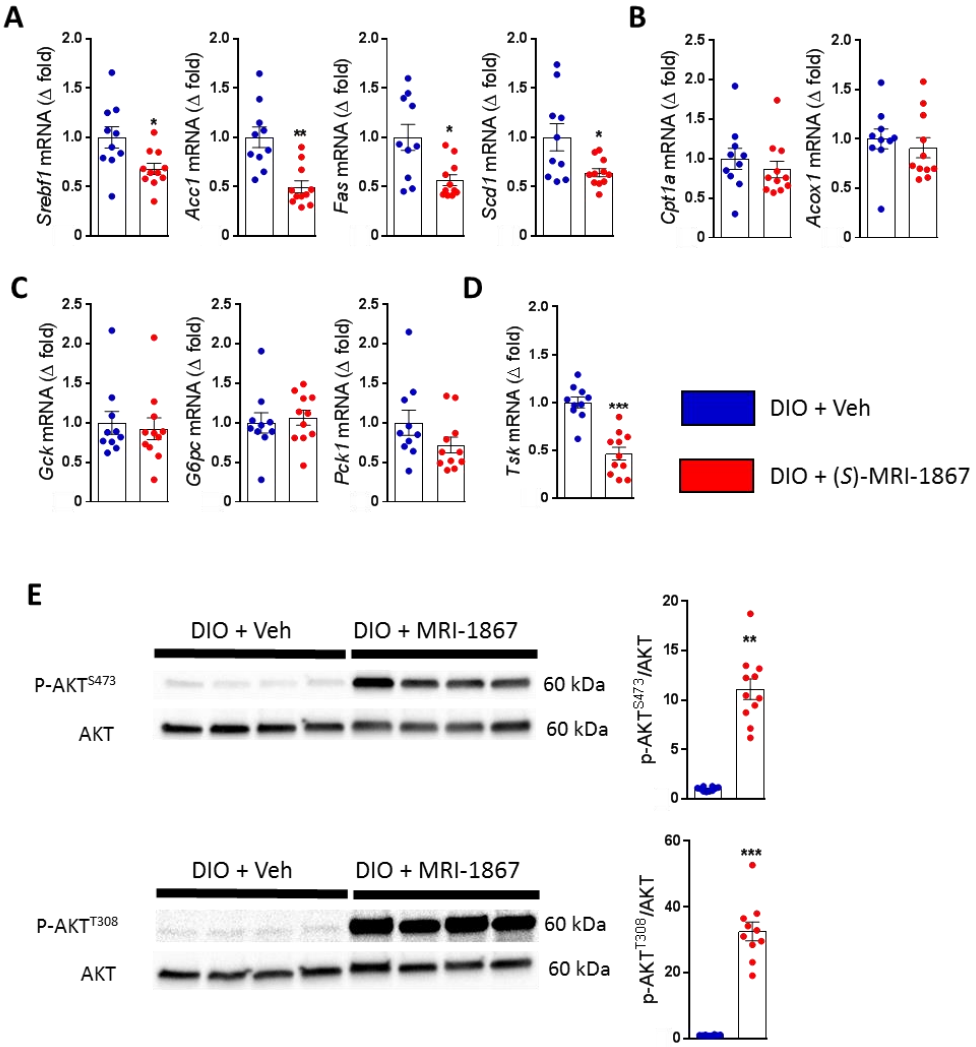

Supplementary Fig. 2: (*S*)-MRI-1867 improves lipid profile by reducing *de novo* lipogenesis without impacting the neoglucogenesis pathway. (A) Gene expression of the *de novo* lipogenic pathway. (B) *Cpt1a* and *Acox1* mRNA levels. (C) *Gck*, *G6pc* and *Pck1* gene expression pattern in the liver. (D) Gene expression level of the hepatokine *Tsk*. (E) Representative immunoblots for ^{S473}- and ^{T308}-phosphorylation of AKT. Blue dots represent the DIO vehicle control mice (n=10) while the red dots represent the DIO *(S)*-MRI-1867 treated mice (n=11). Data represent mean ± SEM. Significance relative to vehicle control: *p<0,05; **p<0,01; ***p<0,001.

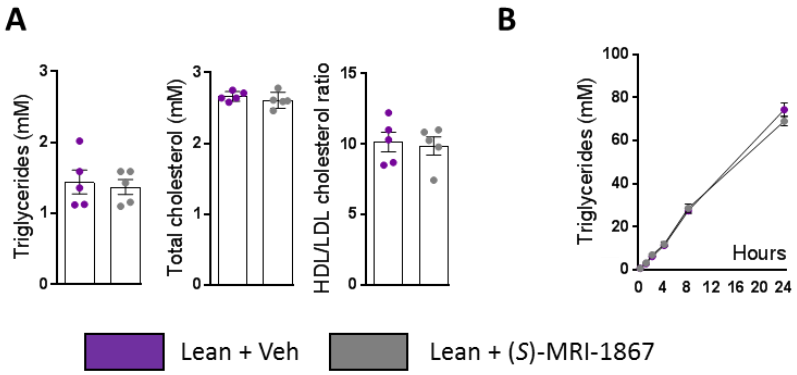

Supplementary Fig. 3: The CB1R blocking action and iNOS inhibitory power of (*S*)-MRI-1867 are regulating different aspect of hepatocyte metabolism in isolated primary hepatocytes. (A) Serum levels triglycerides and total cholesterol levels; HDL-LDL cholesterol ratio. (B) Endogenous hepatic production of triglycerides after LPL inhibition. Purple dots represent the lean vehicle control mice (n=5) while the grey dots represent the lean (*S*)-MRI-1867 treated mice (n=5). Data represent mean ± SEM. Significance relative to vehicle control: *p<0,05; **p<0,01; ***p<0,001.

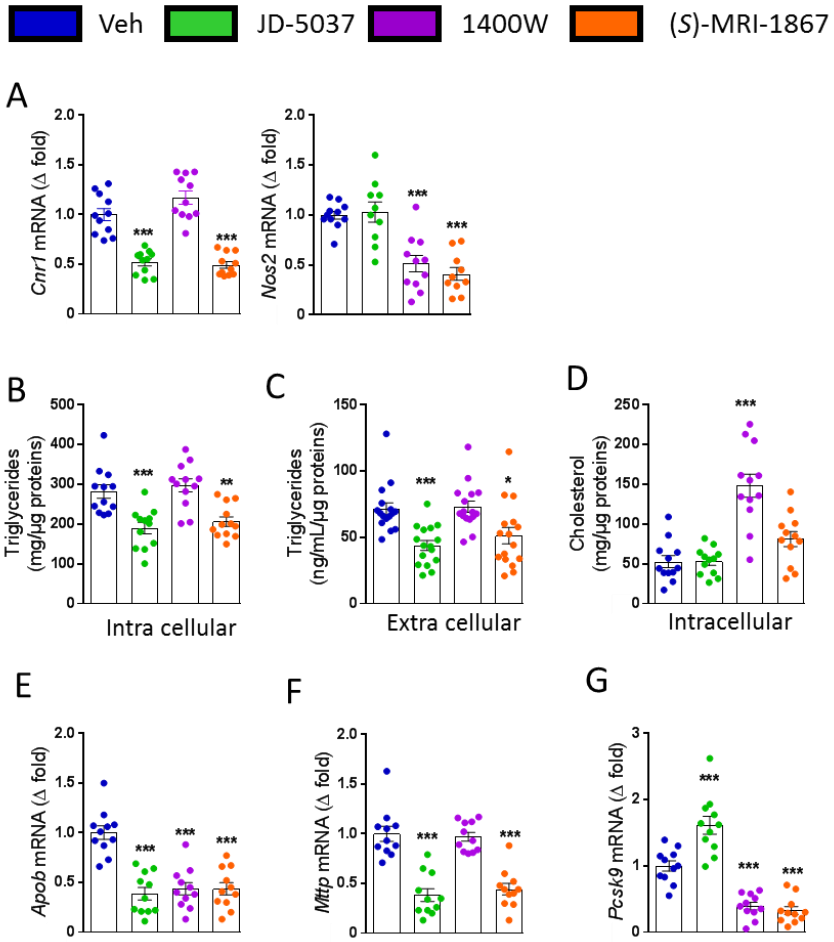

Supplementary Fig. 4: The CB1R blocking action and iNOS inhibitory power of (*S*)-MRI-1867 are regulating different aspect of hepatocyte metabolism in isolated primary hepatocytes. (A) *Cnr1* and *Nos2* expression after 24h treatment. (B) Intracellular triglyceride content after 24h treatment. (C) Measurement of the triglycerides secreted in the culture medium after 24h of treatment. (D) Intracellular cholesterol content after 24h treatment. (E) *Apob* gene expression after 24h of treatment. (F) *Mttp* mRNA levels after 24h of treatment. (G) *Pcsk9* gene expression after 24h of treatment. Vehicle control treatment: DMSO, JD-5037 treatment: 100 nM, 1400W treatment: 10 µM and *(S)*-MRI-1867 treatment: 100 nM. Data represent mean ± SEM from 3-4 independent experiments. Significance relative to vehicle: *p<0,05; **p<0,01; ***p<0,001.

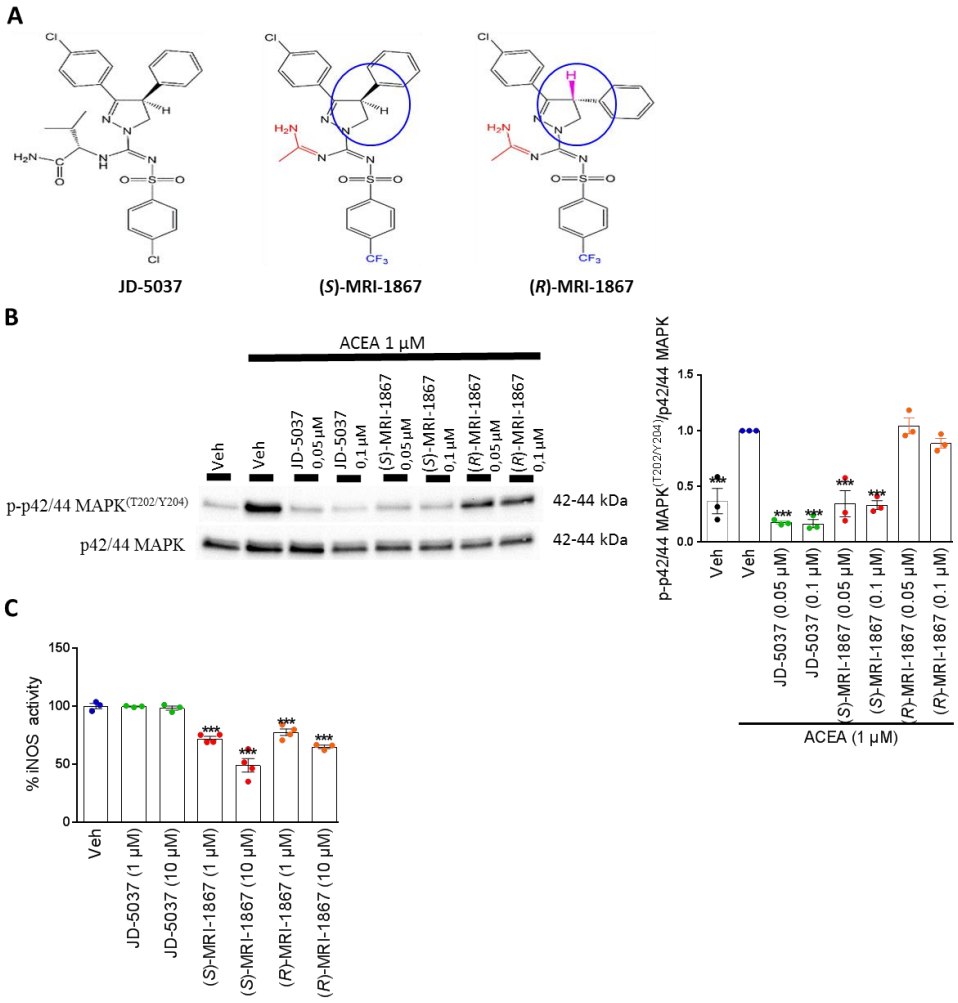

Supplementary Fig. 5: Determination of CB1R blocking and iNOS inhibitory power of JD-5037, (*S*)-MRI-1867 and (*R*)-MRI-1867. (A) Chemical structure of JD-5037, *(S)*-MRI-1867 and *(R)*-MRI-1867. (B) Effects of JD-5037, *(S)*-MRI-1867 and *(R)*-MRI-1867 on ACEA-mediated p42/44 MAPK phosphorylation. Representative blot from 3 independent experiments. (**C**) Effects of *(S)*-MRI-1867 and *(R)*-MRI-1867 on iNOS activity. Data represent mean ± SEM. Significance relative to vehicle control *p<0,05; **p<0,01; ***p<0,001.

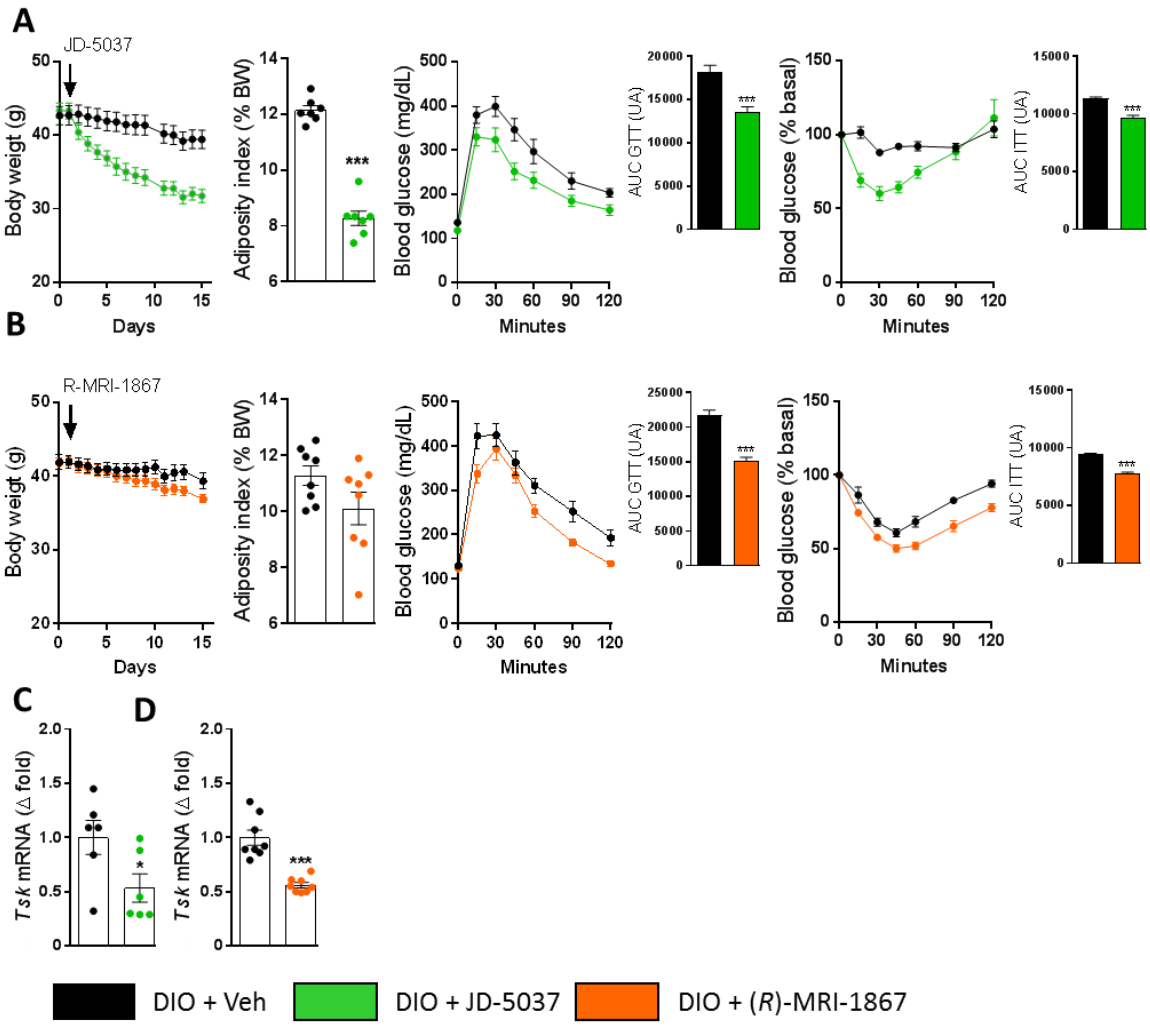

Supplementary Fig. 6: CB1R blockade and Nos2 inhibition show different effects on obesity-related features. (A) Effects of CB1R blockade on body weight, adiposity index, glucose tolerance and insulin sensitivity tests. (B) Effects of iNOS inhibition on body weight, adiposity index, glucose tolerance and insulin sensitivity tests. (C) Effects of CB1R blockade on *Tsk* gene expression. (D) Effects of iNOS inhibition on *Tsk* gene expression. Black dots represent the DIO vehicle control mice (n=6) while the green dots represent the DIO JD-5037 treated mice (n=6). Grey dots represent the DIO vehicle control mice (n=8) while the orange dots represent the DIO *(R)*-MRI-1867 treated mice (n=8). Data represent mean ± SEM. Significance relative to vehicle control *p<0,05; **p<0,01; ***p<0,001.

Supplementary Table 1: list of antibodies used throughout the manuscript

Protein	Species	Dilution	Reference
Phospho-FoxO1^{Ser256}	Rabbit	1/1000	Cell signaling, #84192
FoxO1 (C29H4)	Rabbit	1/1000	Cell signaling, #2880
MTP	Mouse	1/1000	Santa Cruz Biotechnology, sc-515742
LDLR	Goat	1/1000	R&Dsystems, AF2255
SREBP2	Rabbit	1/1000	Abcam, Ab30682
Phospho-mTOR^{Ser2481}	Rabbit	1/1000	Cell signaling, #2974
Phospho-mTOR^{Ser2448}	Rabbit	1/1000	Cell signaling, #5536
mTOR	Rabbit	1/1000	Cell signaling, #2983
RAPTOR	Rabbit	1/1000	Cell signaling, #2280
RICTOR	Rabbit	1/1000	Cell signaling, #2114
Phospho-AKT $^{(S473)}$	Rabbit	1/1000	Cell signaling, #4060
Phospho-AKT $^{(T308)}$	Rabbit	1/1000	Cell signaling, #2965
AKT	Rabbit	1/1000	Cell signaling, #4691
Phospho-p42/44 MAPK$^{(T202/Y204)}$	Rabbit	1/1000	Cell signaling #4377S
p42/44 MAPK	Rabbit	1/1000	Cell signaling #4695S
Anti-Rabbit IgG-HRP	Goat	1/5000	Cell signaling #7074S
HRP-coupled β-actin	Mouse	1/40000	Abcam, Ab49900

All antibodies were diluted in 5% BSA-TBST.

References

[1] Cinar R, Gochuico BR, Iyer MR, Jourdan T, Yokoyama T, Park JK, et al. Cannabinoid CB1 receptor overactivity contributes to the pathogenesis of idiopathic pulmonary fibrosis. JCI insight 2017;2.

[2] Cinar R, Iyer MR, Liu Z, Cao Z, Jourdan T, Erdelyi K, et al. Hybrid inhibitor of peripheral cannabinoid-1 receptors and inducible nitric oxide synthase mitigates liver fibrosis. JCI insight 2016;1.

[3] Tam J, Cinar R, Liu J, Godlewski G, Wesley D, Jourdan T, et al. Peripheral cannabinoid-1 receptor inverse agonism reduces obesity by reversing leptin resistance. Cell metabolism 2012;16:167-179.

[4] Delsal JL. [Extraction and fractionation of serum lipids by previously precipitated serum proteins]. Comptes rendus hebdomadaires des seances de l'Academie des sciences 1957;244:2252-2255.

[5] Degrace P, Demizieux L, Du ZY, Gresti J, Caverot L, Djaouti L, et al. Regulation of lipid flux between liver and adipose tissue during transient hepatic steatosis in carnitine-depleted rats. The Journal of biological chemistry 2007;282:20816-20826.

[6] Millar JS, Cromley DA, McCoy MG, Rader DJ, Billheimer JT. Determining hepatic triglyceride production in mice: comparison of poloxamer 407 with Triton WR-1339. Journal of lipid research 2005;46:2023-2028.

[7] Aparicio-Vergara M, Tencerova M, Morgantini C, Barreby E, Aouadi M. Isolation of Kupffer Cells and Hepatocytes from a Single Mouse Liver. Methods in molecular biology (Clifton, NJ) 2017;1639:161-171.

[8] Muller T, Demizieux L, Troy-Fioramonti S, Gresti J, Pais de Barros JP, Berger H, et al. Overactivation of the endocannabinoid system alters the antilipolytic action of insulin in mouse adipose tissue. American journal of physiology Endocrinology and metabolism 2017;313:E26-e36.

[9] Jourdan T, Godlewski G, Cinar R, Bertola A, Szanda G, Liu J, et al. Activation of the Nlrp3 inflammasome in infiltrating macrophages by endocannabinoids mediates beta cell loss in type 2 diabetes. Nature medicine 2013;19:1132-1140.